CRYSTAL GROWTH & DESIGN

pubs.acs.org/crystal

Article

Why Is α-D-Glucose Monomorphic? Insights from Accurate Experimental Charge Density at 90 K

Luca Sironi, Silvia Rizzato, and Leonardo Lo Presti*

Cite This: *Cryst. Growth Des.* 2022, 22, 6627−6638

Read Online

ACCESS | Metrics & More | Article Recommendations | Supporting Information

ABSTRACT: D-glucose is a strategic chemical for agri-food and pharma industries, which are now exploiting an expected increase of 5% in the global investment round from 2020 to 2028. Despite such a broad industrial interest, the reasons behind room-p monomorphism in D-glucose are unclear. The crystal structure of α-D-glucose is provided here with an unprecedented resolution (0.46 Å) by single-crystal X-ray diffraction at T = 90(1) K. Occurrence of anomeric disorder in the α phase, which has not been reported to date, is demonstrated. The topological analysis of the total charge density distribution is also carried out within the framework of Bader's Quantum Theory of Atoms in Molecules, allowing to rank the relative strength of hydrogen bonds in the crystal structure. It is found that most OH···O contacts have a significant covalent character and build up an exceptionally stiff three-dimensional hydrogen bond network. On the one hand, this locks the molecular conformation by hampering the rotational flexibility of the hydroxy substituents. On the other hand, favorable recognition modes, based on the interaction of the charge density distributions of glucose molecules, cooperatively account for the lattice cohesion. A change in the relative orientation of OH groups would affect the crystal cohesion by changing locally the molecular electrostatic potential, $V(\mathbf{r})$.

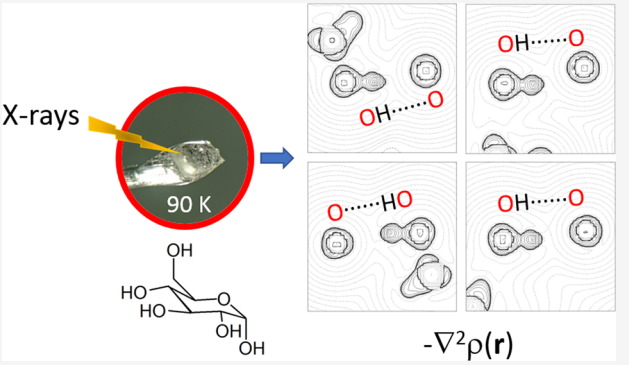

INTRODUCTION

D-glucose (dextrose, $C_6H_{12}O_6$) is a chemical of widespread use in foods, cosmetics, and pharmaceutical formulations. The global glucose market was valued at almost 45 billion USD in 2021,[1] and the demand is expected to grow due to stricter regulations in additives for products intended for human consumption.[2] D-glucose is also employed as a basic scaffold for the synthesis of drugs[3] and other chemicals, including ascorbic acid and sorbitol.[4] Despite such a broad interest, some important aspects of solid-state chemistry of D-glucose are still open to investigation, as testified by recent contributions on its high pressure behavior[5] and relative phase stability.[6]

In aqueous solution, D-glucose is mainly present in the pyranose cyclic form[7] as a mixture of α and β anomers (Figure 1). These are involved in an acid-catalyzed dynamic equilibrium ("mutarotation") that results in a 40:60 α/β ratio at 30 °C.[7] The β form prevails due to a more favorable hydration energy of ∼1.7 kcal·mol^{-1},[8] but the equilibrium mixture progressively enriches in α at higher T.[7] To date, three crystal forms of D-glucose are known,[9−15] and a fourth one is produced by the rearrangement of H bonds in the anhydrous α structure above 5.40(2) GPa.[5] According to Young,[16] the monohydrated α polymorph ($P2_1$) can be crystallized from diluted aqueous solutions (up to 50% w/w) at moderate temperature (T < 50 °C), while higher T's and concentrations are generally required to obtain the orthorhombic $P2_12_12_1$ anhydrous α (T > 50 °C, w/w > 50%) and β (w/w > 80%) forms (Figure 1).

The α-monohydrated form is the least soluble at low T and can be easily obtained, for example, by slow evaporation at room T. Increasing both temperature and concentration favors the anhydrous forms, which can be obtained by slow cooling of concentrated solutions; crystalline β prevails at very high concentrations (Figure 1).

As other metabolites of low molecular weight,[17−19] D-glucose is highly functionalized, with five easily rotatable[20] −OH groups and one endocyclic oxygen, all available for hydrogen bonds. Moreover, the pyranose ring can adopt chair, boat, and skew-boat conformations, all accessible in standard ambient conditions.[21] Thus, it might be surprising that no conformational polymorphs of D-glucose are known to date.[8,22] On the computational side, the rotational flexibility of −OH groups in pyranose sugars produces several low energy structures.[23−25]

With the only exception of the high-p phase,[5] no polymorphs of anhydrous α-D-glucose were reported to date,

Received: July 26, 2022
Revised: October 10, 2022
Published: October 20, 2022

https://doi.org/10.1021/acs.cgd.2c00846
Cryst. Growth Des. 2022, 22, 6627−6638

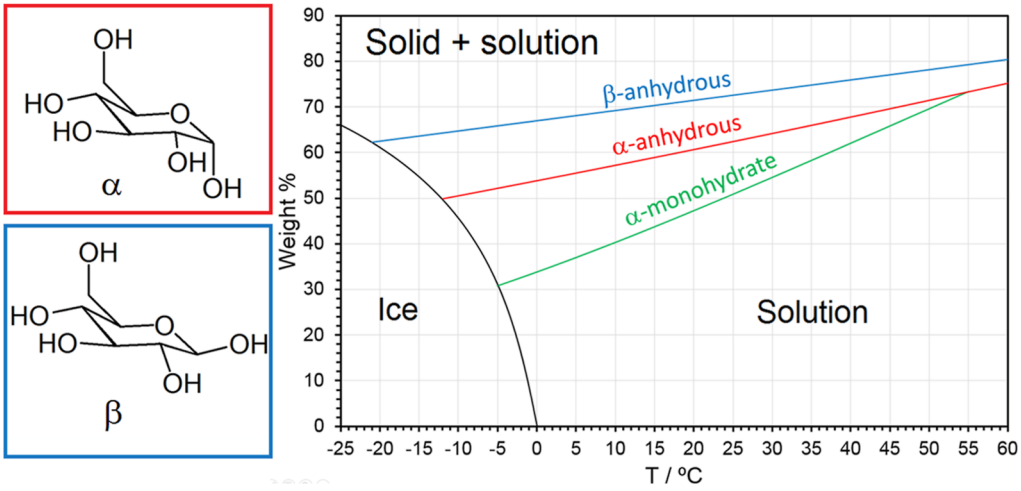

Figure 1. Left: α and β anomers of D-glucose. Right: composition/temperature phase diagram of the water/glucose system at p° = 1 bar. Solubility curves are based on Young's interpolation of experimental solubility data.[16]

despite extensive and large-scale crystallizations carried out daily worldwide. To shed light on (room-p) monomorphism in glucose, a deep and quantitative knowledge of the main intermolecular recognition modes is mandatory. We here report on a high-resolution (0.46 Å) solid-state study of α-D-glucose by means of single-crystal X-ray crystallography at T = 90(1) K. The purpose is to study self-recognition of the title compound by using the magnifying lens provided by the experimental charge density distribution. To this end, real-space topological descriptors of chemical bonding were employed within the framework of Bader's Quantum Theory of Atoms in Molecules (QTAIM).[26] Not only do we rank the OH···O hydrogen bonds according to their relative strength, but we also resolve the occurrence of previously unreported anomeric disorder. Results provide insights on monomorphism of the title compound.

METHODS

Synthesis of α-D-Glucose Crystals. Reagent-grade chemicals were purchased by Aldrich and used without further purification. A programmable Huber CC-205B heating circulation thermostat equipped with a Compatible Control was employed to carry out slow-cooling crystallizations. Three flat bottom test tubes (ϕ 16 mm) each containing 1.0 mL of 78.5% w/w solution of α-D-glucose in Milli-Q water were put into a jacketed reactor. After 30′ conditioning at 70.0 °C, the temperature was lowered to 55.0 °C under a linear gradient of 1.0 °C/hour. Nucleation occurred at 55.7−56.0 °C, as spotted by visual inspection. These conditions ensure that crystallization occurs when a full α−β anomeric equilibrium is set up in solution, based on literature kinetic measurements.[7] An X-ray quality specimen (Table 1) was cut from a larger aggregate using a stainless steel microblade and polished by mechanical ablation in a drop of perfluorinated oil. The crystal was mounted on top of a glass capillary fiber with two-component epoxy glue.

X-ray Data Collection and Reduction. X-ray data collections were carried out at T = 90(1) K up to a resolution of 0.46 Å ($\sin\theta/\lambda_{MAX}$ = 1.09 Å^{-1}, Table 1) with a three-circle Bruker AXS SMART diffractometer equipped with an Apex II CCD detector and an Oxford Cryosystems N_2 gas blower. Diffraction intensities were recorded in ω-scan mode with graphite-monochromated Mo Kα radiation (λ = 0.71073 Å), using a normal focus sealed tube at a nominal power of 50 kV × 30 mA.

The data were integrated by Bruker SAINT+,[27] while SADABS[27] was employed to scale and correct empirically the recorded intensities for beam anisotropy and absorption. The structure was solved by direct methods with SIR92[28] and initially refined with SHELX[29] under the independent atom model (IAM) approximation. The final model included occupational disorder of substituents at the anomeric carbon, with the site occupation factor (s.o.f.) of the minority

Table 1. α-D-Glucose: Crystallographic Data for the 90(1) K Study

sample information		
empirical formula	$C_6H_{12}O_6$	
formula wt/g mol^{-1}	180.156	
crystal system	orthorhombic	
space group	$P2_12_12_1$	
Z	4	
crystal dimensions/mm	0.500 × 0.150 × 0.100	
T/K	90(1)	
a/Å	10.317(2)	
b/Å	14.822(3)	
c/Å	4.9338(10)	
V/Å^3	754.5(3)	
D_i/g cm^{-3}	1.586	
F(000)	384	
absorption coeff. μ/mm^{-1}	0.144	
data collection		
cryostat	N_2 gas blower	
λ/Å	0.71073	
$(\sin\theta/\lambda)_{max}$/Å^{-1}	1.09	
scan technique	ω-scan	
scan rate (ω)/° min^{-1}	1.5−0.5	
ω−scanrange/°	180	
no. collected refln.s	78 286	
no. unique refln.s	8182	
no. obsd refln.s ($I > 0$, N_{obs})	8105	
R_{int}	0.0352	
least-squares refinements		
	spherical atom refinement	multipole refinement
$R(F)$	0.0343	0.0233
$wR(F^2)$	0.0883	0.0545
goodness-of-fit	1.039	0.9839
$\Delta\rho_{max}/\Delta\rho_{min}$/$e$·Å^{-3}	0.58(7)/-0.22(7)	0.28(4)/-0.23(4)
spherical ($\zeta = \kappa\alpha$) and deformation ($\zeta' = \kappa'\alpha'$) atomic exponents/Bohr^{-1}		C: 1.008(4)/0.876(12), H: 1.25(2)/1.36(5), O: 0.977(2)/1.20(3)

https://doi.org/10.1021/acs.cgd.2c00846
Cryst. Growth Des. 2022, 22, 6627−6638

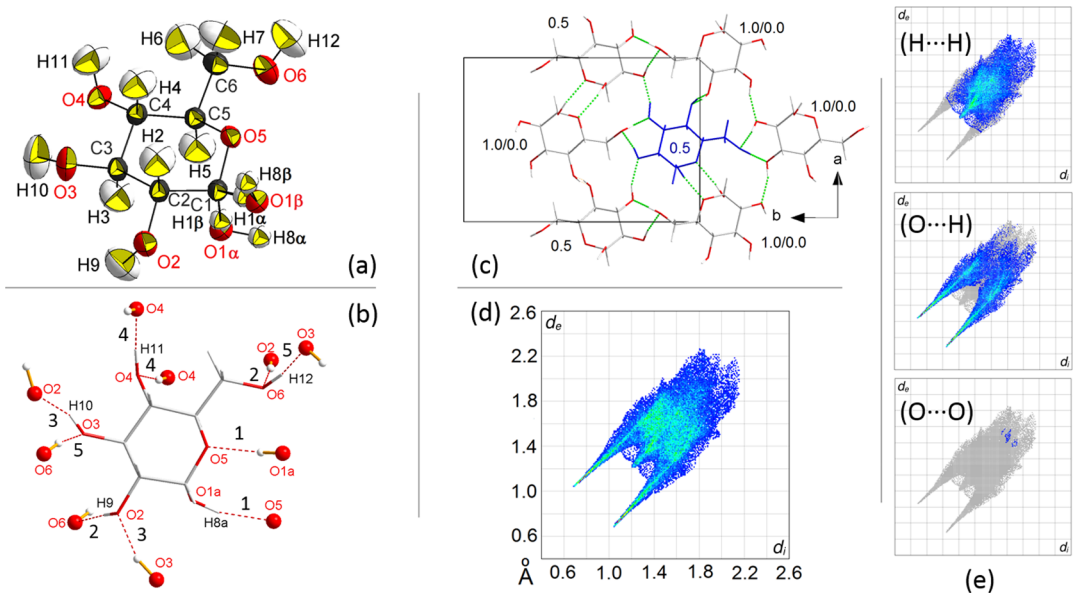

Figure 2. (a) Asymmetric unit of anhydrous α-D-glucose at T = 90(1) K, with the atom numbering scheme. Thermal ellipsoids were drawn at the 95% probability level. Substituents at the anomeric carbon C1 are disordered, with s.o.f.'s of 0.96 (α) and 0.04 (β). (b) OH···O hydrogen bond map of the α anomer. Each interaction has an identifying label according to Table 1. See Section S4 in Supporting Information for the β anomer. (c) Crystal packing of anhydrous α-D-glucose in the (a,b) plane. The hydrogen bond network is highlighted as dotted green lines (asymmetric unit in blue). The height along c of each molecule is also given in fractional coordinates. (d) Hirshfeld surface fingerprint plot of the α anomer. The analogue plot including contributions from the β anomer is shown in Section S4 Supporting Information. (e) Fingerprint plot coverage for different classes of atom−atom contacts.

conformer refining to 0.055(3) (see below). Such disorder was modeled by positioning two H atoms from the difference map and introducing the other two in calculated positions.

Experimental Charge Density. The total experimental charge density distribution of the title compound, $\rho(\mathbf{r})_{exp}$, was extracted from a 99.8% complete set of 8182 symmetry-independent structure factor amplitudes in the framework of the Hansen−Coppens multipole formalism[30] by using the XD2016 program package.[31] The multipole expansion was based on the Clementi and Roetti functions.[32] The least-squares matrix was solved with the Gauss−Jordan algorithm, using an eigenvalue cutoff limit of 10^{-9} and a convergence criterion of 10^{-6} on the maximum error-weighted parameter shift. All the observed reflections (I > 0) were included in the refinement.

The complexity of the least-squares model was increased stepwise (full details in Section S1 in the Supporting Information). C−H and O−H covalent distances were restrained to average neutron estimates of Allen and Bruno.[33] The thermal motion of H atoms was modeled as anisotropic with the TLS + U procedure implemented in the SHADE2.1 web server[34,35] and kept fixed thereinafter. The final multipole expansion included hexadecapoles (l = 4) for C, O, and quadrupoles (l = 2) for H atoms. Radial scaling parameters κ and κ' for each atomic species were also refined. The disorder at the anomeric carbon (see above) was handled by (*i*) not refining the s.o.f.'s of the involved atoms at the best SHELX estimate; (*ii*) imposing a general restraint of equal total charges for the coexisting α and β molecules; (*iii*) truncating the multipole expansion to l = 2 and 1 for disordered O and H atoms; (*iv*) refining a unique set of thermal and multipole parameters for the disordered O and H atoms. Final agreement factors and other relevant quantities are shown in Table 1.

The topological analysis of the $\rho(\mathbf{r})_{exp}$ scalar field was carried out with the XDPROP routine embedded in XD2016.[31] Both local (critical points) and nonlocal (integral) properties were evaluated by the study of the gradient field in the real space. As for integral properties, up to 50 × 3470 points were employed for the radial (Gauss−Legendre) and angular (Lebedev) quadrature, with a target accuracy in surface determination of 10^{-3} Å. A fifth-order Runge−Kutta integrator was employed to solve ordinary differential equations in the $\rho(\mathbf{r})$ field. Some atoms (C4−C6, H1α, H7, H10, and H12) showed poor accuracy, and their integral properties were extrapolated to zero Lagrangian according with the procedure described elsewhere.[36,37] Eventually, the quality of the integration was highly satisfactory, with an average Lagrangian as low as 5.1 × $10^{-5}e$·Å^{-2} and the sum of total integrated charges not exceeding an absolute unbalance of 3 × $10^{-3}e$.

Bulk Quantum Simulations. Periodic quantum calculations were carried out by CRYSTAL17[38] on an error- and disorder-free model of the α-D phase, exploiting the PBE0/pob-TZVP-rev2 level of theory.[39,40] The Fourier transform of the DFT charge density gave a set of synthetic structure factor amplitudes (F_{theo}), which in turn were employed to develop a multipole density, $\rho(\mathbf{r})_{theo}$, fully comparable with the $\rho(\mathbf{r})_{exp}$ distribution. A complete discussion can be found in Section S2 in Supporting Information.

Molecular Dynamics Simulations of the Crystal. Classical simulations were carried out with the MiCMoS 2.0 program suite, exploiting both the Coulomb−London−Pauli (CLP) and Lennard−Jones−Coulomb (LJC) force fields embedded in the source code.[41−46] 1.0 ns-long *NPT* trajectories at time steps of 2 fs were run at 90 K and ambient pressure. The simulation box consisted of 3 × 2 × 7 crystallographic unit cells with 168 α-D-glucose molecules and an approximately cubic shape (31.1 × 29.7 × 34.8 Å^3). Box dimensions and shape were selected to ensure that relevant collective lattice vibrations are accounted for in all directions, as testified by the substantial agreement among experimental and predicted lattice parameters. Full details are deposited in Section S3 in Supporting Information.

Gas Phase Quantum Simulations. Single-point SCF calculations on isolated molecular pairs extracted from the crystal at their final multipole geometry (see above) were carried out at the perturbative MP2/6-311G* level of theory as implemented in Gaussian 16.[47] The purpose was to estimate the pair cohesive energy. The basis set superposition error (BSSE) was accounted for by the counterpoise procedure by Boys and Bernardi.[48]

Reproducibility. Input XD files and full experimental structure factor amplitudes in *.hkl* and *.fcf* format were deposited in Supporting Information. Relevant input files used in quantum and classical simulations are documented in Sections S2 and S3 in Supporting

https://doi.org/10.1021/acs.cgd.2c00846
Cryst. Growth Des. 2022, 22, 6627−6638

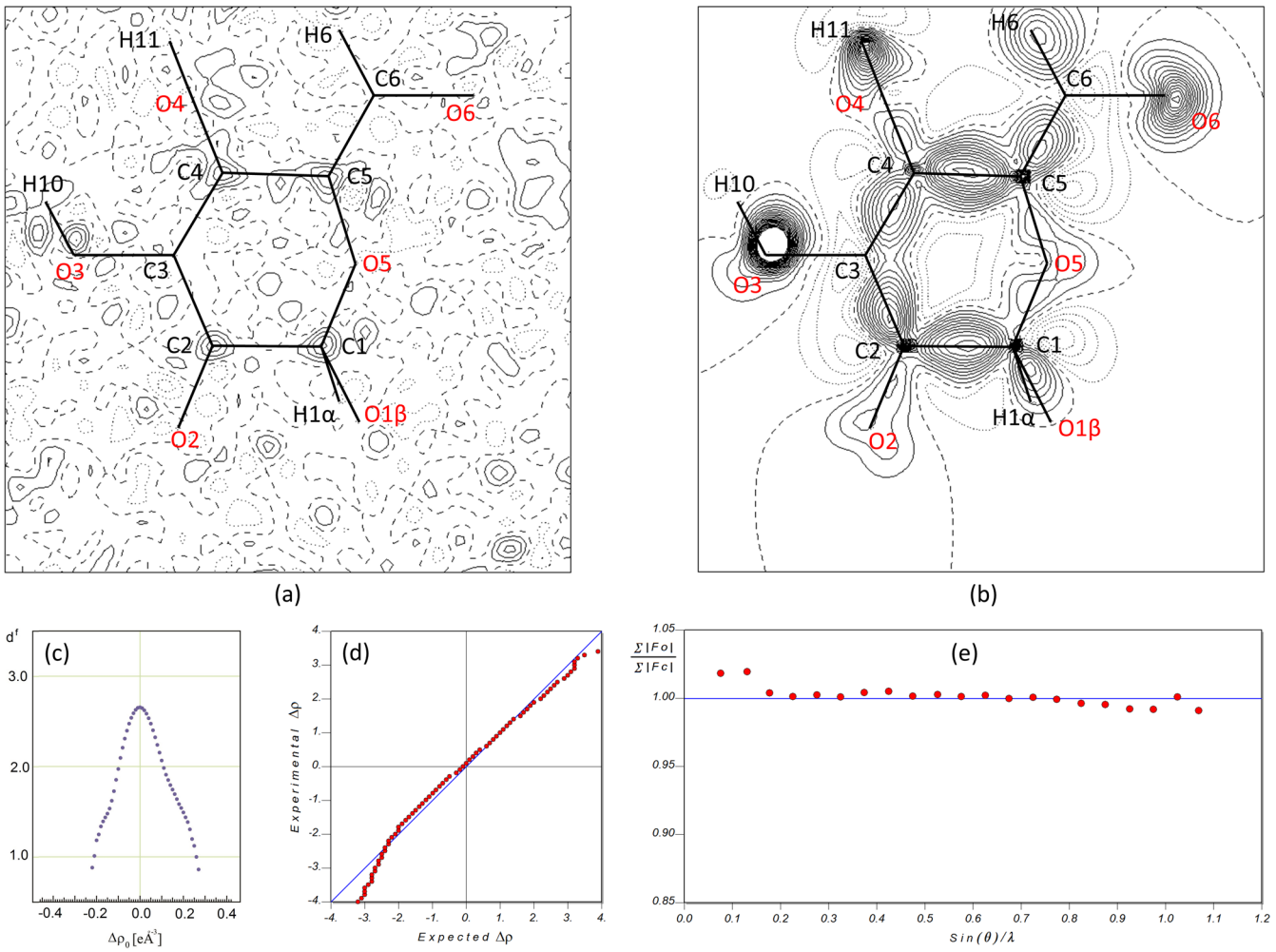

Figure 3. Quality of experimental charge density model of α-D-glucose at 90 K. Contour levels in both graphs (a) and (b) are drawn at steps of 0.05 e·Å^{-3} in a 8 × 8 Å wide plane containing atoms C1, C2, C4, and C5 (full lines: positive, dotted lines: negative, dashed lines: $\Delta\rho$ = 0 contours). (a) Difference Fourier density map ($\Delta\rho$) in the crystal. (b) Static deformation density map. (c) Distribution of Hausdorff fractal dimension for the experimental residual charge density. (d) Normal probability plot of $\Delta\rho$ residuals. (e) Average ratio of summed F_{hkl}^{o} and F_{hkl}^{c} as a function of sinθ/λ. The closer it is to 1, the better the model reproduces the F_{hkl}^{o}'s in each sinθ/λ shell. Deviations are <2.5% and much lower in most cases.

Information. CCDC 2192771 contains the supplementary crystallographic data for this paper. These data can be obtained free of charge from the Cambridge Crystallographic Data Centre via www.ccdc.cam.ac.uk/structures.

RESULTS

Anomeric Disorder. Least-square IAM refinements of the α-D-glucose structure against the high-resolution data set at 90(1) K invariably led to odd results in the anomeric region: the anomeric hydrogen H1 had a negative isotropic displacement parameter; the C1−H1 bond distance was abnormally long (1.21(2) Å), and a significant Fourier residual of +0.56 e·Å^{-3} was present along the bond, lying at 0.610 Å from C1. Any attempt to go on with a multipole refinement resulted in a positively (negatively) charged O1 (H1) atom, strongly suggesting the occurrence of some extra electron density contributions close to H1. In retrospect, the warnings sketched above were already present in a standard preliminary IAM refinement against RT data at the Cu-sphere resolution, though they were so poorly evident that they went totally unnoticed. The issue was solved by introducing anomeric disorder in the IAM model, which resulted in an estimated population of 5.5(3)% for the β form. The improvement in the overall agreement factors was significant according to the Hamilton test[49] (see Section S4 in Supporting Information). Starting from the IAM estimate for the s.o.f.'s of anomeric substituents, we tested several multipole models and finally we selected a value of 4.0% for the β form, which was optimal on the basis of $wR(F)$, $wR(F^2)$, goodness-of-fit, and Fourier difference residues (Figure 2a).

We do not claim that anomeric disorder was present throughout the crystallization batch, as we did not carry out extensive sampling. Future studies could aim at establishing whether disorder is common within the α phase, and whether α and β anomers may co-crystallize in specific conditions. A take-home message is that disorder involving low-occupancy light atoms could be difficult to recognize in standard data sets collected at room temperature, as it might be easily confused with anharmonicity[50,51] or even go unnoticed when absorbed into apparently large harmonic thermal parameters. Synergy of high resolution and low temperature[51,52] proves to be highly desirable to provide accurate structure determinations of molecular crystals.

Crystal Structure of α-D-Glucose at 90(1) K. The title compound crystallizes in the chiral apolar acentric $P2_12_12_1$

https://doi.org/10.1021/acs.cgd.2c00846
Cryst. Growth Des. 2022, 22, 6627−6638

Table 2. Strong Intermolecular OH···O Contact in the α-D-Glucose Crystal at T = 90(1) K, from the Multipole-Level Geometry. All Symmetry-Independent Contacts with $d_{H\cdots O} \leq 3.0$ Å, $120° \leq \alpha_{OHO} \leq 180°$ are Included[a]

contacts (O−H···O)	#	symmetry[b]	O−H/Å	H···O/Å	O···O/Å	α_{OHO}/°
O1α−H8α···O5	1	1/2 − x, −y, −1/2 + z	0.97	1.90	2.8268(7)	158
O2−H9···O6	2	1 − x, 1/2 + y, 1/2 − z	0.97	1.79	2.7492(7)	171
O3−H10···O2	3	1/2 + x, 1/2 − y, 1 − z	0.97	1.75	2.6841(7)	161
O4−H11···O4	4	3/2 − x, −y, 1/2 + z	0.97	1.80	2.7758(7)	169
O6−H12···O3	5	1 − x, −1/2 + y, 3/2 − z	0.97	1.74	2.6962(8)	168

[a]Sensible estimated standard deviations are reported in parentheses. [b]According to standard solid-state conventions, symmetry codes refer to acceptor atoms.

space group (no. 19) with four molecules in the unit cell and one (α/β-disordered) molecule in the asymmetric unit (Table 1, Figure 2a). The amount of β anomer is minoritarian (4%). Thus, crystal packing is neatly dominated by α−α contacts, and the presence of β can be safely considered as a perturbation of the main interaction network (see below and Section S4 in Supporting Information). Accordingly, direct β−β contacts are unlikely.

Glucose molecules adopt an almost perfect chair conformation, with the pyranose ring exhibiting a puckering amplitude[53] of 0.5711 Å, and configurational polar coordinates θ = 4.24° and φ = 318.38° for the sequence O5−C1−C2−C3−C4−C5. The asymmetric unit is involved in allegedly strong HB interactions with 10 screw-related neighbor molecules, of which only 5 are symmetry-independent (Figure 2 and Table 1 and Figure S3 and Table S3 in Supporting Information). Four out of five hydroxy groups act as donors and acceptors of OH···O hydrogen bonds, with the only exception of the anomeric one (O1−H8), which only binds the pyranic O5 acceptor.

No cyclic H-bonded molecular pairs are present. Rather, a complex three-dimensional network is formed, where each glucose moiety acts as a node connecting 10 neighboring molecules on three contiguous layers at fractional heights of 0.0, 0.5, and 1.0 along c (Figure 2c). The crystallographic unit cell corresponds to the minimal volume that accounts for the space occupied by this 11-molecule cluster, which is tightly connected to its translation-related images in neighboring cells.

The paramount importance of close HB contacts in this structure is also highlighted by the Hirshfeld surface fingerprint plot[54,55] (Figure 2d), which is dominated by a couple of parallel spikes ending at $(d_i + d_e)_{min} \approx 1.7$ Å due to OH···O contacts. The latter account for roughly one-half (48.7%) of the Hirshfeld surface coverage, while H···H contacts account for the 51.1% (Figure 2e). Such a large H···H coverage is due to very short OH···O HBs, which get H atoms close to each other. The remaining 0.2% is due to O···O contacts, localized in the upper right part of the fingerprint (Figure 2e). These evidences point out that, from a geometrical viewpoint, intermolecular interactions are invariably mediated by the OH groups. More accurate insights on molecular recognition require to study mechanical stability and interaction energetics, as discussed in the next sections.

Total Experimental Charge Density. The quality of the present experimental charge density determination is testified by the essentially featureless Fourier difference maps (Figure 3a). We note that positive residues of $\Delta\rho(\mathbf{r})$, not exceeding +0.2 e·Å^{-3}, are visible on some C atoms of the glucopyranose ring. They are probably imputable to still unresolved disorder, possibly dynamic in nature,[51] even though it is difficult to reach safe conclusions considering the unavoidable correlations of disorder with structural and electronic parameters. Further experimental work at higher resolution and lower T is required to solve the issue. In any case, the static deformation map is consistent with the features expected in a six-membered ring containing sp^3-hybridized carbon atoms (Figure 3b). The fractal distribution of the charge density residuals, $d^f(\Delta\rho)$,[56,57] has also the expected behavior (Figure 3c). d^f quantifies how much specific $\Delta\rho$ isosurfaces can spread through the whole space; the closer $d^f(0)$ is to 3, the closer is the $\Delta\rho$ = 0 isosurface to cover the three-dimensional Euclidean manifold.

For the present data set, the distribution peaks sharply around 0 with $d^f(0)$ = 2.65, which is comparable with other estimates in recent charge density studies of our group.[51,58] Moreover, maximum $\Delta\rho$ does not exceed ±0.28 e·Å^{-3} and reduces to ±0.1 e·Å^{-3} in the fractal d^f = 2 manifold, a parameter that is taken as a robust estimator of the model quality.[51] A small deviation from the ideal bell-shaped curve is appreciable at higher $|\Delta\rho|$'s, which mirrors in a deviation from linearity of the lower tail of the normal probability plot (Figure 3d) and is likely related to the residual positive Fourier peaks discussed above on C atoms. This might suggest a small residual overfitting, which is to be expected due to the difficulty of disentangling disorder, thermal motion, and valence population parameters, especially in the anomeric region of the molecule. However, we note also that the normal probability plot is reasonably linear around $\Delta\rho$ = 0, and that the average agreement among observed (F_{hkl}^o) and predicted (F_{hkl}^c) structure factor amplitudes is highly satisfactory (Figure 3e). As expected, maximum and minimum residuals [+0.28(4) and −0.23(4) e·Å^{-3}] are in the disordered region, close to O(1A) and O(1B). Overall, the final least-squares model catches all the relevant features of the charge density distribution embedded in measured structure factor amplitudes. The substantial agreement of charge density-derived properties, like the HB energies and electrostatic potential (see below), among the multipole models based on F_{theo} and F_{exp} further confirms the quality of the present data set. Overall, the experimental picture of chemical bonding in the OH···O regions is reasonably accurate, as testified by the good agreement with benchmark computational models (see *infra*).

Intermolecular Cohesion. Comparison of accurate experimental structures of α-D-glucose, including the present one, shows that the torsions involving hydroxy groups do not change in the 90−300 K range of T (Table S4 Supporting Information). T-dependent MD simulations with the LJC force field[44] further confirm these results. This suggests that the torsional degrees of freedom are locked in a tightly bonded arrangement, resulting in a rigid network that is scarcely influenced by temperature. Also, hydrogen bond distances and angles are strictly conserved on cooling down to 90 K (Table S5 in Supporting Information). This is also in accordance with

https://doi.org/10.1021/acs.cgd.2c00846
Cryst. Growth Des. 2022, 22, 6627−6638

Table 3. E_{int} and E_{HB} of Symmetry-Independent Relevant Molecular Pairs (see Figures 2 and S4 Supporting Information) Extracted from the Crystal, as Computed by Either Quantum (MP2 6-31G) or Classical (Static Atom−Atom LJC) Methods on the Final Multipole-Level Geometry[a]**

			AA-LJC[d]				E_{HB}			
#	d_{CM}/Å[b]	QM[c] E_{int}	E_{dis}	E_{coul}	E_{rep}	E_{int}	ρ_{exp}[e]	ρ_{theo}[f]	BD_{exp}[g]	BD_{theo}[g]
1	5.805	−36.7	−31.2	−24.1	11.4	−43.9	−27(3)	−24.1	0.25	0.30
2	7.815	−17.8	−20.9	−13.3	9.5	−24.7	−36(16)	−40.5	−0.28	−0.12
3	7.446	−19.2	−26.7	−14.9	12.4	−29.3	−53(16)	−47.5	−0.28	−0.13
4	6.343	−23.2	−28.1	−18.8	11.1	−35.8	−35(14)	−40.8	−0.12	−0.11
5	7.820	−19.0	−33.7	−18.9	16.3	−36.3	−30(15)	−50.3	−0.03	−0.16

[a]All values in kJ·mol^{-1}. [b]Molecular center of mass distance. [c]MP2-level quantum mechanical E_{int} corrected for BSSE by the counterpoise method.[48] [d]Static atom−atom calculations with the classical LJC functional embedded in MiCMoS.[46] E_{dis}, E_{coul}, and E_{rep} are dispersion, coulomb, and repulsive contributions to E_{int}. [e]Hydrogen bond energy estimated from local topological descriptors of the experimental charge density (eq 1−3). Estimated standard deviations (e.s.d.'s) in parentheses. The e.s.d. of #1 is apparently lower due to least-squares constraints and lower-order multipole expansion applied to disordered anomeric atoms (see the Methods section). [f]Hydrogen bond energy estimated from local topological descriptors of the multipole-projected theoretical charge density (eq 1−3). [g]Bond degree parameter, BD = $H(\mathbf{r})_{bcp}/\rho(\mathbf{r})_{bcp}$, where $H(\mathbf{r})$ is the total energy density. Units of hartree·e^{-1}.

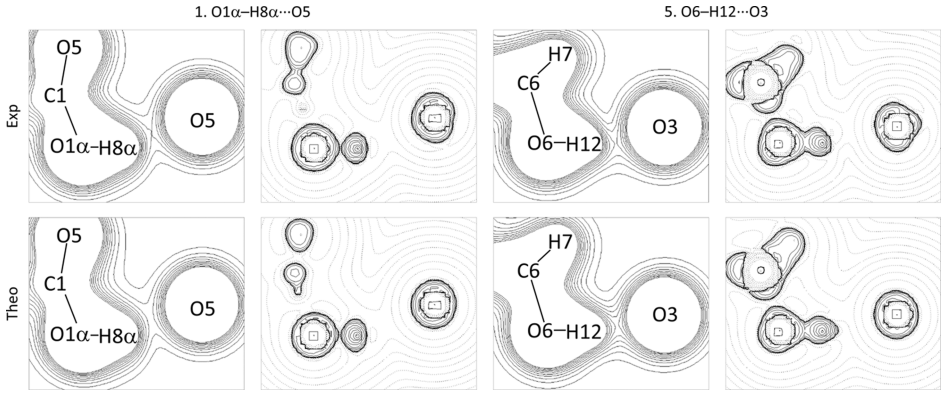

Figure 4. Charge density and negative charge density Laplacian isolevels in the O1α-H8α···O5 (left) and O6−H12···O3 (right) HB planes in crystalline α-D-glucose at T = 90(1) K, as obtained from the experimental (first row) and theoretical (second row) $\rho(\mathbf{r})$ distributions. These two HBs were chosen as they represent the extreme points of the spanned energy range (Table 3 and Figure 5). Laplacian maps of the other HBs are shown in Figure S6, Supporting Information. Charge density isolevels were drawn from 0 to 0.50 at steps of 0.05 in units of e·Å^{-3}, while variable step intervals of $\pm a \cdot 10^{-n}$ were employed for the Laplacian in units of e·Å^{-5} (a = 9.64, 4.82, and 2.20 and n = 0, ±1, ±2, ±3, ±4, and ±5). Dotted lines: $\nabla^2\rho > 0$; dashed lines: $\nabla^2\rho = 0$; full lines: $\nabla^2\rho < 0$.

the fact that the average volume thermal expansion coefficient of D-glucose (α_V = 7(2)·10^{-5} K^{-1}, this work) is roughly one-half of the generally expected in organic crystals (α_V = 1.7(7)·10^{-4} K^{-1}).[59] The small change in cell volume upon cooling (Figure S5, Supporting Information) strongly suggests a fully harmonic behavior of the lattice (Einstein-like). No evidence of anharmonic motion was present, at variance of organic compounds whose cohesive forces are dominated by non-directional (or poorly directional) physical interactions.[50,51,58,60]

To gain insights into the most important recognition modes (Table 3), we followed a twofold strategy. First, we evaluated the BSSE-corrected pair interaction energies (E_{int}) of molecules connected by symmetry-independent OH···O interactions at the MP2 level of theory. E_{int}'s quantify the total (i.e., nonlocal) stabilization energy of each molecular pair extracted from the crystal with respect to the same non-interacting molecules. Second, we focused on local estimates of the hydrogen bond energies, E_{HB}, which do not necessarily correlate with E_{int}.[19,61−63] We evaluated E_{HB}'s by MiCMoS LJC classical atom−atom summations on the experimental X-ray structure. These came at no computational cost and provide a straightforward analysis of dispersive, Coulomb, and repulsive terms, under the assumption that many-body terms are negligible. Moreover, E_{HB}'s can be obtained from the analysis of real-space local topological descriptors of the experimental (ρ_{exp}) and multipole-projected (ρ_{theo}) charge densities (see the Methods section). We exploited Abramov's functional[64] to estimate the kinetic energy density ($G(\mathbf{r})_{bcp}$) from the charge density and charge density Laplacian at the bond critical point (bcp)

$$G(\mathbf{r})_{bcp} = \frac{3}{10}(3\pi^2)^{2/3}\rho(\mathbf{r})_{bcp}^{5/3} + \frac{1}{6}\nabla^2\rho(\mathbf{r})_{bcp} \quad (1)$$

Equality (1) is based on Kirzhnitz-corrected Thomas−Fermi expression for the electron kinetic energy[64] and is applicable in low $\rho(\mathbf{r})$ regions when $\nabla\rho = 0$, like the HB's bcp. Then, the local form of the virial theorem is applied to evaluate the potential energy density at the bcp

$$V(\mathbf{r})_{bcp} = \frac{\hbar^2}{4m}\nabla^2\rho(\mathbf{r})_{bcp} - 2G(\mathbf{r})_{bcp} \quad (2)$$

where m is the mass of the electron. Following Espinosa,[65] a good descriptor of E_{HB} for strong hydrogen bonds[66] is the functional

$$E_{HB} = \frac{1}{2}V(\mathbf{r})_{bcp} \quad (3)$$

https://doi.org/10.1021/acs.cgd.2c00846
Cryst. Growth Des. 2022, 22, 6627−6638

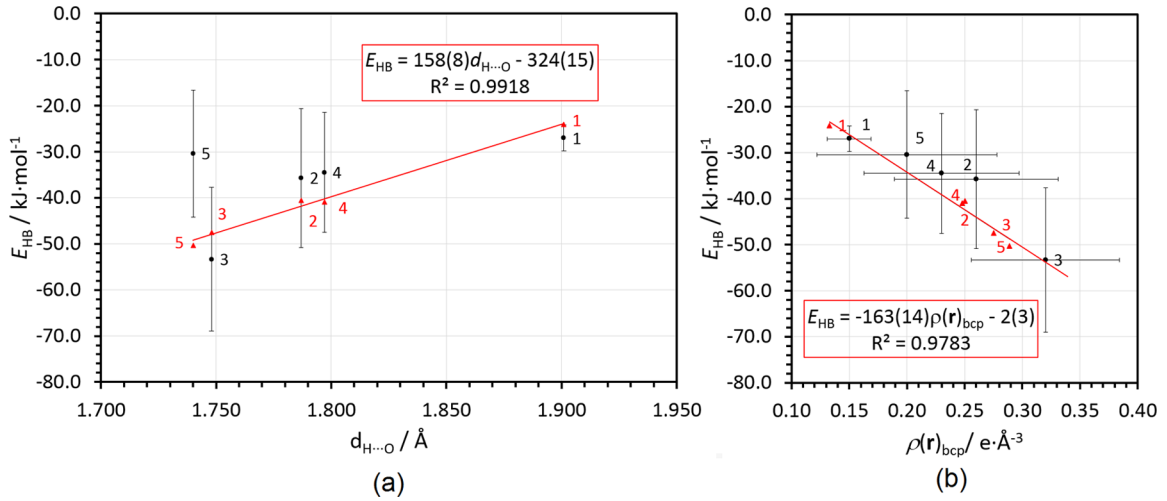

Figure 5. (a) E_{HB}, as evaluated according to eq 3, versus $d_{H\cdots O}$ for symmetry-independent HB contacts in α-D-glucose at T = 90(1) K. Red triangles: estimates from the multipole-projected charge density distribution, ρ_{theo}. The red line is the corresponding linear regression, with relevant statistical parameters shown in the highlighted box. Black rhombi: estimates from the experimental charge density distribution, ρ_{exp}. Vertical error bars correspond to 1 least-squares e.s.d. (b) Same E_{HB}'s as in (a) versus the charge density at the bcp. Linear regression from ρ_{theo} data in red. Error bars correspond to 1 e.s.d.

As expected, all HBs are characterized by positive Laplacian values, but potential energy prevails in most of them (#2−5, Table 3), resulting in a negative total energy density, $H(\mathbf{r}) = V(\mathbf{r}) + G(\mathbf{r})$. From the virial eq 2, this implies that $G(\mathbf{r}) < V(\mathbf{r}) < 2\ G(\mathbf{r})$; that is, such bonds are associated with a certain amount of electron sharing and are not purely electrostatic in nature. This can be also appreciated by looking at Laplacian contours in the OH···O plane of representative hydrogen bonds (Figure 4). A neat polarization of the valence shell charge concentration region of the H basin along the direction of the H···O bond can be appreciated for O6−H12···O3 (#5). The same is also true for #2−4 HBs (Figure S6, Supporting Information), while no bond-directed polarization can be recognized at all along the anomeric H8α···O5 (#1) interaction.

Switching to energies, a comparison of experimental E_{HB}'s with periodic DFT-derived ones gives similar results (Figure 5a). A neat linear relationship (R^2 > 0.99) is evident among HB energies and H···O distances in the ρ_{theo} distribution, as the amount of charge density at the bcp increases linearly with the formal bond order for shared (or partly shared) chemical bonds (Figure 5b, Table S6 Supporting Information).[26] This is consistent with the fact that we are inspecting at a very narrow distance window (∼1.8−1.9 Å), where the exponential trend found by Espinosa[65] can be reasonable approximated with a linear function. Owing the small magnitude of the charge density and its Laplacian in the internuclear region (<0.4 e·Å^{-3}, ≤ +3 e·Å^{-5}), even small model inaccuracies may result in very large relative errors, making the extraction of reliable chemical information from the observed structure factor amplitudes a difficult business.

First, it is worth noting that the only HB whose geometry is markedly different from the others is #1 (1.90 Å, 158°), which is consistently predicted as the least stable one by all the computational methods and bears only electrostatic character (Table 3). The other hydrogen bonds #2−5 all have more negative E_{HB} (Table 3) and are very similar from a geometrical viewpoint (Table 2). Their H···O distances range from 1.74 to 1.80 Å and are identical to their average (1.77(1) Å) within 3 e.s.d.'s. The variance of angles is higher (average: 167(2)°, range: 161−171°), but no patent correlations can be found with the E_{HB} energies. For example, the most acute angle (#3) is always associated with a very strong HB, while #5 is predicted to be the strongest one by the ρ_{theo} topology, although it bears an OHO angle essentially identical to #2 and #4. A possible take-home message is that the HB stability is mainly determined by the electronic features of the interaction (i.e., electrostatic or partly covalent), which in turn determine the resulting geometry.

Most importantly, the E_{HB} estimates from the ρ_{exp} distribution follow the same trend as those predicted from ρ_{theo}, namely, $|E_{HB}(3)| > |E_{HB}(2)| \approx |E_{HB}(4)| > |E_{HB}(1)|$, even though the large e.s.d.'s make the differences among them poorly significant. Considering the occurrence of disorder at the anomeric carbon C1 (see above), such conformity of views is noteworthy and confirms that the quality of the experimental charge density analysis is high enough to draw safe conclusions on this system, albeit on a qualitative level. The ρ_{exp} topology significantly underestimates the stability of the fifth bond, O6−H12···O3 [1 − x, −1/2 + y, 3/2 − z] (Table 3, Figures 4 and 5). The latter turns out to have E_{HB} close to those of bonds 2 and 4, while it should be the most stable one on absolute grounds, based on the ρ_{theo} prediction. The reason of this discrepancy can be traced back in a ≈33% large underestimation of the charge density at the bcp (Figure 5b), which results in a less positive $G(\mathbf{r})$ (eq 1) and a less negative $V(\mathbf{r})$ henceforth (eq 2). We note that the anomeric H8···O5 interaction (# 1), which is totally electrostatic in nature ($\nabla^2\rho$ > 0, BD > 0), is not affected and is satisfactorily modeled by both ρ_{theo} and ρ_{exp} distributions.

Comparison of total interaction energies (E_{int}) and hydrogen bond energies (E_{HB}) in Table 3 reveals that there is a general inverse correlation between them: the more negative is E_{int}, the less E_{HB}. In other words, the most strongly bonded molecular dimers are connected by the weakest HBs.

This does not imply that OH···O interactions are weak on absolute grounds: on the contrary, E_{HB}'s in glucose are comparable in magnitude with those found in charge-assisted HBs in organic salts[19] and neatly more negative than those estimated in natural compounds of similar composition and

https://doi.org/10.1021/acs.cgd.2c00846
Cryst. Growth Des. 2022, 22, 6627−6638

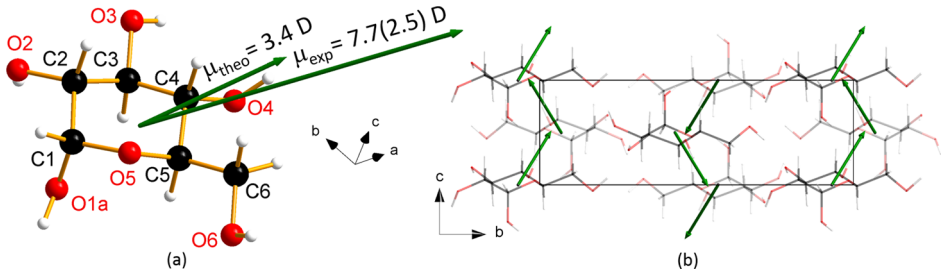

Figure 6. (a) Experimental and theoretical dipole moments of α-D-glucose extracted from the crystal, referred to the molecular center of mass. The corresponding magnitudes are displayed, together with the relative orientation of the molecular with respect to the crystallographic cell axes. Arrows point toward the negative ends of each dipole. (b) Packing of molecular dipoles, seen down the *a*-axis.

Table 4. Dipole Moment Module and Components (All Quantities in Debye, in the Cartesian Reference Frame with the Origin on the Molecular Center of Mass) of α-D-Glucose for Different Models Employed in This Work[a]

model	partitioning	μ_x	μ_y	μ_z	$\|\mu\|$
ρ_{exp}	HC DMA[b]	3.2 ± 1.5	−4.6 ± 1.7	5.2 ± 0.9	7.7 ± 2.5
	QTAIM[c,d]	3.2 ± 0.8	−4.6 ± 1.1	5.2 ± 0.6	7.6 ± 1.7
ρ_{theo}	HC DMA[b]	1.9	−1.5	2.4	3.4
	QTAIM[c]	1.9	−1.5	2.4	3.4

[a]Experimental e.s.d.'s are also given. [b]Hansen−Coppens distributed multipole analysis. [c]QTAIM partitioning of the charge density. Each component μ_i of the total molecular dipole moment was computed according to $\mu_i = \sum_j [q_j r_{ij} + \mu_{ij}]$, where the summation runs across the j atoms in the asymmetric unit and $i = x, y, z$. r_{xj}, r_{yj}, and r_{zj} are positions of atom j with respect to the molecular center of mass, q_j is the integrated charge of atom j, and μ_{ij} expresses the atomic dipolar deformation along x, y, and z, as estimated from the momenta of the charge density distribution within the atomic basin j. [d]E.s.d.'s are based on an estimated average standard deviation of $2.5 \times 10^{-2}e$ on the integral charge.

weight.[17,67] This result is not surprising, as molecular interaction energies are intrinsically multi-body in origin and depend on how the two whole charge density distributions interact.[62] A take-home message is that care should be paid when one tries to rank atom−atom interactions based on pure E_{int} estimates. As for the present case, large negative E_{int}'s are invariably associated with the largest electrostatic contributions, as estimated by the classical LJC force field. This further highlights the importance of electrostatics in anhydrous glucose, as polar molecules ($|\mu|$ = 2.8 D, in vacuo PBE0 estimate) tend to arrange into favorable head-to-tail interactions under the constraint of null cell dipole moment imposed by the 222 point symmetry of the crystal (see also Figure 6 in the next section).

To gain insights into the role of the β anomer in the α structure, we computed BSSE-corrected MP2-level E_{int} estimates of the same symmetry-independent hydrogen bonded pairs here discussed, where the HB donor is the β molecule. This resulted in 5 direct β−α contacts (Table S7 Supporting Information), the probability of β−β interactions being negligible due to the low amount of β in the α matrix (see above). A new allegedly strong HB (#1b) is now set up with the O6 hydroxy of the molecule at $1/2 - x, -y, 1/2 + z$ (Section S4, Supporting Information), with the corresponding pair accounting for E_{int} = −49.8 kJ·mol^{-1} (Table S7, Supporting Information). At the same time, the O1−H8···O5 HB (#1) is broken, while all the other E_{int}'s in the cluster become slightly more negative. This is noteworthy, as the O2−O6 hydroxy groups conserve the same geometry and, therefore, local properties of hydrogen bonds #2−5 are expected to be conserved as well. The average stability gain in electronic potential energy amounts to −1.4(3) kJ·mol^{-1} per molecular pair, summing up to a total gain of −5.8 kJ·mol^{-1} for the symmetry-independent molecule−molecule interactions. Discussing the effect of anomeric disorder on the stability of the crystal would require the quantitative estimation of entropic contributions, which are out of reach for our in vacuo static quantum simulations. However, the following points are worth of note: (*i*) substitution of one β molecule determines a more favorable (negative) BSSE-corrected E_{int} in all neighboring α−β pairs and (*ii*) anomeric disorder can only add favorable entropy contributions, implying a further decrease of the chemical potential of the system. In other words, both terms (enthalpic and entropic) determine a stability gain, that is, substitution of α with β increases the cohesion of the whole HB cluster. The implications are twofold: (*i*) the very low concentration of the β anomer in the α matrix must be ascribed just to the lower solubility of the α phase at moderate heating (Figure 1). In turn, this implies that the occurrence of anomeric defects in the α lattice may not be occasional. Extensive screening with high-resolution data sets on different crystal batches should be carried out to verify this hypothesis. (*ii*) The overall attractive potential in the HB cluster is not attributable just to strong HBs. Molecule−molecule interactions involving their whole charge density distributions also play a role, as a change in the orientation of the only anomeric −OH is enough to produce a significant change in E_{int} within the cluster, when all the individual molecule−molecule contributions are accounted for. To gain insights on this matter, the total electrostatic potential of D-glucose is discussed in the next section.

Electrostatics. Multipolar Hansen−Coppens and QTAIM integral atomic charges are quite different (Tables S9 and S10, Supporting Information). This is expected, owing to the different partitioning schemes on which they rely. Pseudoatom multipoles have no boundaries: they decrease asymptotically beyond the van der Waals radius, that is, they are free to overlap. QTAIM charges, on the other hand, are obtained by integrating the $\rho(\mathbf{r})$ distribution over nonoverlapping atomic basins bound by surfaces that satisfy the zero-flux conditions of

https://doi.org/10.1021/acs.cgd.2c00846
Cryst. Growth Des. 2022, 22, 6627−6638

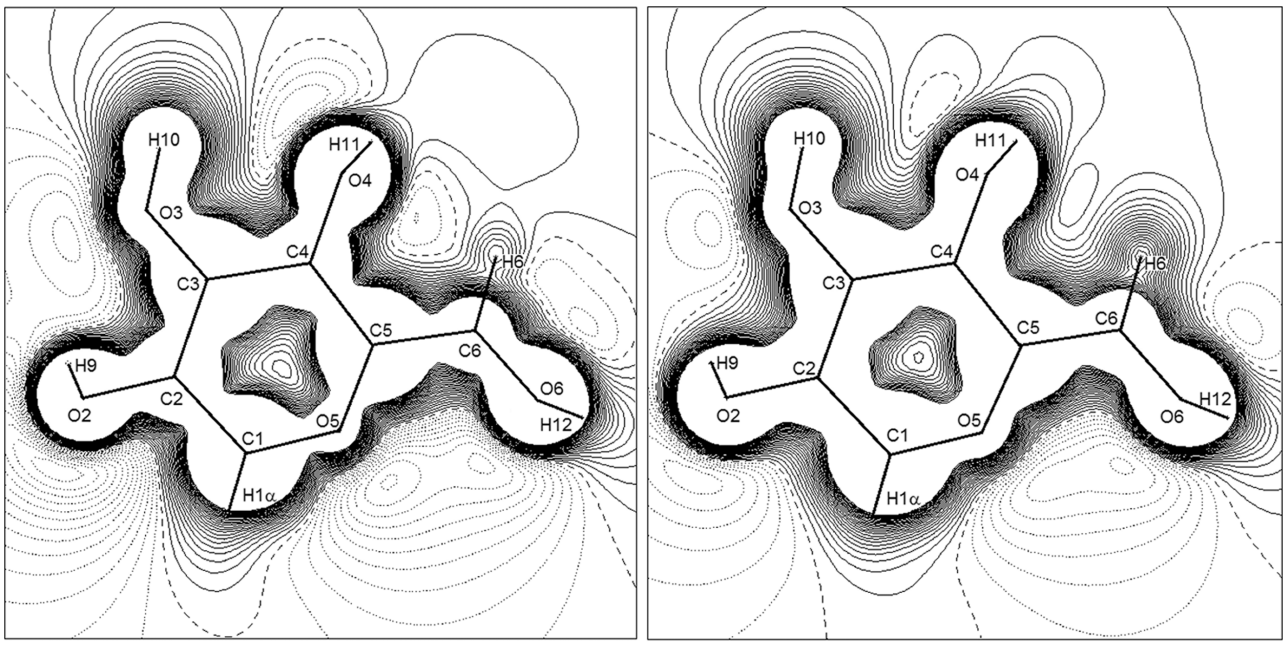

Figure 7. Electrostatic potential, $V(\mathbf{r})$, for the α-D-glucose molecule extracted from the crystal in the plane defined by atoms O2−O6−O4, as obtained from the experimental charge density ρ_{exp} (a) and from the multipole-projected one ρ_{theo} (b). Both maps are 8.9 × 8.9 Å wide, and contour levels are drawn at steps of 0.02 $e{\cdot}Å^{-1}$. Dotted lines: $V(\mathbf{r}) < 0$; dashed lines: $V(\mathbf{r}) = 0$; solid lines: $V(\mathbf{r}) > 0$. More specific maps in relevant HB planes are shown in Section S6 Supporting Information.

the $\nabla\rho$ field, $\oint \nabla\rho(r)\bullet\hat{n}dS = 0$. The integration of atomic basins thus depends on the choice of the atomic boundaries, which are necessarily different if the crystal or the isolated molecule is considered. If the atomic zero-flux surfaces are moved to infinity, both the partitioning schemes should provide the same estimate for electrostatic observables, like the molecular dipole moment. This is indeed the case (Table 4 and Figure 6).

Contrasting values are given for the dipole moment of α-D-glucose in the literature. Oliveira[68] reported 4.3 D in the gas phase and 5.3 D in solution at the MP2/6-311++G(2d,2p) level of theory, as compared with our own prediction of 2.8 D obtained from the accurate 90 K molecular geometry at the PBE0/pob-TZVP-rev2 level. These large differences likely reflect conformational differences in the D-glucopyranose moiety, as isolated molecules set up intramolecular OH···O hydrogen bonds, which are not present in the crystal. Other computational predictions are also available (2.5 D).[69] In contrast, the popular Wikipedia page on D-glucose reports a suspiciously high (and unreferenced) value of 8.7 D.[70] To the best of our knowledge, the present charge density-based estimate (Table 4) provides the only *experimental* data available for the dipole moment of α-D-glucose. It is worth noting that the ρ_{exp} and ρ_{theo} distributions substantially agree in the dipole direction, with a deviation not exceeding ≈12° (Figure 6). The dipole magnitude is probably overestimated by ρ_{exp}, as the error-free multipole refinement on the theoretical structure factors gives a roughly halved value. However, the very large uncertainty associated with ρ_{exp} makes the difference barely significant on statistical grounds, as the two modules are equal within less than 2 e.s.d.'s. Diffraction experiments at the liquid He temperature, possibly on anomerically pure crystals, are required to improve the precision and accuracy of the charge density-derived electrostatics. However, our best estimate for the in-crystal dipole moment enhancement (from 2.8 to 3.4 D, +21%) is perfectly comparable with that predicted by Oliveira and Colherinhas[68] in solution (+23%).

A look at the electrostatic potential, $V(\mathbf{r})$, roughly in the mean molecular plane (Figure 7), allows us to gain further insights on electrostatics and hence on what are the expected preferential interaction modes of molecules with themselves. Negative isolevels imply a prevalence of negative charges and are associated with regions of valence charge concentration, like those stemming from the lone pairs of oxygen atoms. There is a good qualitative agreement between the experimental and theoretical multipole models. However, ρ_{exp} overestimates the charge separation with respect to ρ_{theo}, in agreement with the unphysical enhancement of the dipole vector module discussed above. Interestingly, both models predict a large bay area of negative potential in the region of O5 and O6 lone pairs. This area is responsible for the observed direction of the molecular dipole, which goes out-of-plane with a large component along the crystallographic direction *c* (Figure 6). Moreover, due to chemical constraints imposed by the sp^3 hybridization of oxygen atoms, a pattern of highly structured zones of positive and negative $V(\mathbf{r})$ arises around the pyranose ring. Regions of large positive electrostatic potential spread from the O−H bonds (Figure 7) and interact in a key-lock fashion with large negative zones close to oxygen acceptors of neighboring molecules (e.g., H10···O2, H12···O3—see Figures 2b and 7). These evidences confirm that cohesion in α-D-glucose stems from the synergy of directional strong OH···O HBs with favorable electrostatic interactions spanning the crystal lattice (Figure 6b).

CONCLUSIONS

In this work, a high-resolution (0.46 Å) single-crystal X-ray diffraction study was carried out at 90(1) K on the anhydrous

https://doi.org/10.1021/acs.cgd.2c00846
Cryst. Growth Des. 2022, 22, 6627−6638

α anomer of D-glucopyranose. The purpose was to understand why conformational polymorphism was never observed to date at room pressure, despite the very low rotational barriers of the exocyclic −OH groups. To this end, we extracted the accurate charge density distribution, $\rho(\mathbf{r})$, from the observed structure factor amplitudes, studying relevant intermolecular interactions with the topological toolbox provided by the QTAIM. Both classical and quantum simulations were also carried out to complement the experimental picture and validate the accuracy of the main results with suitable error-free models.

Synergy of low temperature and high resolution demonstrated the occurrence of previously unreported anomeric disorder. We found that the β form accounts for 4% of the total unit cell content, and we confirmed that its inclusion is energetically favored. More extensive studies are required to understand to what extent anomeric disorder is frequent in α-D-glucose crystals. This issues a warning on the importance of working with reliable high-resolution data to characterize accurately organic crystals containing only light atoms, especially when different equilibrium species coexist in the crystallization liquor.

The α-D-glucose lattice was poorly affected by cooling, according to the low measured isobaric thermal expansion coefficient. The relative orientation of hydroxy groups did not change down to 90 K. The topological analysis of the $\rho(\mathbf{r})$ distribution confirmed the high stiffness of the HB network: 4 out of 5 OH···O close contacts have a neat partial covalent character. This is due to the significant polarization of the valence shell charge concentration of hydrogen atoms toward their oxygen acceptors, appreciable also from the $-\nabla^2\rho(\mathbf{r})$ maps. At the same time, a key-lock superposition of highly structured $V(\mathbf{r}) < 0$ and $V(\mathbf{r}) > 0$ bay areas around the pyranose ring accounts for directional OH···O interactions. This mirrors in generally very large HB energies, E_{HB}.

Perhaps counterintuitively, we found an inverse correlation between total molecule−molecule interaction energies (E_{int}) and E_{HB}. Directional HBs tell us just a part of the story: the lattice cohesion also stems from advantageous electrostatic contributions among molecular $\rho(\mathbf{r})$ distributions, for example, head-to-tail arrangement of dipole moments. Indeed, substitution of the α anomer with β implies that E_{int} of each neighboring molecular pair becomes more negative even though the geometry of partially covalent OH···O bonds remains unchanged.

To conclude, in contrast to the large conformational variability of isolated α-D-glucose molecules, possible occurrence of conformational polymorphism in the solid state is hampered by two factors: (*i*) the exceptional stiffness of the HB network, as partially covalent OH···O hydrogen bonds set up very stable intermolecular cooperative interactions, and (*ii*) favorable key-lock interactions among electron-rich and electron-poor regions of electrostatic potential of neighboring molecules. Any change in the mutual orientation of −OH groups, despite setting up almost equivalent HB interactions on geometrical grounds,[23−25] would affect the electrostatic potential, resulting in a loss of cohesion of the whole translation-independent molecular cluster (Figure 2). A strong evidence supporting this hypothesis is the significant change in E_{int}'s of α−β pairs, whose OH···O contacts are not affected by anomeric substitution.

A final remark concerns the applicability of classical force fields when electrostatics and quantum (partial covalence) effects are intertwined. *Ad hoc* parametrization should be normally required to mimic such a borderline physics, and the lucky success of the LJC force field is likely due to extensive parametrization against properties of polar/HB liquids and crystals.[44]

■ ASSOCIATED CONTENT

Supporting Information

The Supporting Information is available free of charge at https://pubs.acs.org/doi/10.1021/acs.cgd.2c00846.

Details of the experimental multipole model, multipole-projected theoretical charge density, molecular dynamics, crystal packing: contribution of the β anomer, intermolecular recognition, electrostatic properties, and deposited files: input XD files and full experimental structure factor amplitudes in *.hkl* and *.fcf* format (PDF)

Accession Codes

CCDC 2192771 contains the supplementary crystallographic data for this paper. These data can be obtained free of charge via www.ccdc.cam.ac.uk/data_request/cif, or by emailing data_request@ccdc.cam.ac.uk, or by contacting The Cambridge Crystallographic Data Centre, 12 Union Road, Cambridge CB2 1EZ, UK; fax: +44 1223 336033.

■ AUTHOR INFORMATION

Corresponding Author

Leonardo Lo Presti − *Department of Chemistry, Università degli Studi di Milano, 20133 Milano, Italy; Istituto Nazionale di Fisica Nucleare (INFN), Laboratori Nazionali di Frascati, Frascati 00044, Italy;* orcid.org/0000-0001-6361-477X; Email: leonardo.lopresti@unimi.it

Authors

Luca Sironi − *Department of Chemistry, Università degli Studi di Milano, 20133 Milano, Italy;* orcid.org/0000-0003-2839-4243

Silvia Rizzato − *Department of Chemistry, Università degli Studi di Milano, 20133 Milano, Italy; Istituto Nazionale di Fisica Nucleare (INFN), Laboratori Nazionali di Frascati, Frascati 00044, Italy;* orcid.org/0000-0001-9893-0238

Complete contact information is available at: https://pubs.acs.org/10.1021/acs.cgd.2c00846

Notes

The authors declare no competing financial interest.

■ REFERENCES

(1) Glucose Market Size, Share | Industry Report, 2020-2028https://www.grandviewresearch.com/industry-analysis/global-glucose-market (accessed June 28, 2022).

(2) The Worldwide Glucose Industry is Expected to Reach $63.6 Billion by 2028https://www.prnewswire.com/news-releases/the-worldwide-glucose-industry-is-expected-to-reach-63-6-billion-by-2028--301384173.html (accessed June 27, 2022).

(3) Halmos, T.; Santarromana, M.; Antonakis, K.; Scherman, D. Synthesis of O-Methylsulfonyl Derivatives of d-Glucose as Potential Alkylating Agents for Targeted Drug Delivery to the Brain. Evaluation of Their Interaction with the Human Erythrocyte GLUT1 Hexose Transporter. *Carbohydr. Res.* **1997**, *299*, 15−21.

(4) Alves, L. A.; Almeida e Silva, J. B.; Giulietti, M. Solubility of D-Glucose in Water and Ethanol/Water Mixtures. *J. Chem. Eng. Data* **2007**, *52*, 2166−2170.

(5) Patyk, E.; Katrusiak, A. Transformable H-Bonds and Conformation in Compressed Glucose. *Chem. Sci.* **2015**, *6*, 1991−1995.
(6) Chihi, T.; Ghebouli, M. A.; Fatmi, M. Predictive Physical Study of Two Different Crystalline Forms of Glucose. *Biochem. Biophys. Rep.* **2021**, *25*, 100923.
(7) Le Barc'H, N.; Grossel, J.; Looten, P.; Mathlouthi, M. Kinetic Study of the Mutarotation of D-Glucose in Concentrated Aqueous Solution by Gas-Liquid Chromatography. *Food Chem.* **2001**, *74*, 119−124.
(8) Schnupf, U.; Willett, J. L.; Momany, F. DFTMD Studies of Glucose and Epimers: Anomeric Ratios, Rotamer Populations, and Hydration Energies. *Carbohydr. Res.* **2010**, *345*, 503−511.
(9) Fronczek, F. R.*Experimental Crystal Structure Determination*; CSD Communication, 2016 (Private Communication.
(10) Mostad, A.; Neumann, K.; Larsen, S.; Wang, D.-N.; Springborg, J.; Paulsen, G. B.; Nielsen, R. I.; Olsen, C. E.; Pedersen, C.; Stidsen, C. E. X-Ray Crystallographic Study of Alpha-Glucose at 140 K. *Acta Chem. Scand.* **1994**, *48*, 276−278.
(11) Brown, G. M.; Levy, H. A. α-D-Glucose: further refinement based on neutron-diffraction data. *Acta Crystallogr., Sect. B: Struct. Crystallogr. Cryst. Chem.* **1979**, *35*, 656−659.
(12) Ferrier, W. G. The crystal and molecular structure of β-D-glucose. *Acta Crystallogr.* **1963**, *16*, 1023−1031.
(13) Chu, S. S. C.; Jeffrey, G. A. The refinement of the crystal structures of β-D-glucose and cellobiose. *Acta Crystallogr., Sect. B: Struct. Crystallogr. Cryst. Chem.* **1968**, *24*, 830−838.
(14) Kouwijzer, M. L. C. E.; Van Eijck, B. P.; Kroon, H.; Kroon, J. An extension of the GROMOS force field for carbohydrates, resulting in improvement of the crystal structure determination of α-D-galactose. *Acta Crystallogr., Sect. B: Struct. Sci.* **1995**, *51*, 209−220.
(15) Dean, G. R. Optical-crystallographic properties of .beta.-D-glucose. *Anal. Chem.* **1973**, *45*, 2440−2441.
(16) Young, F. E. D-Glucose-Water Phase Diagram. *J. Phys. Chem.* **1957**, *61*, 616−619.
(17) Lo Presti, L.; Soave, R.; Destro, R. On the Interplay between CH···O and OH···O Interactions in Determining Crystal Packing and Molecular Conformation: An Experimental and Theoretical Charge Density Study of the Fungal Secondary Metabolite Austdiol (C12H12O5). *J. Phys. Chem. B* **2006**, *110*, 6405−6414.
(18) Saleh, G.; Soave, R.; Lo Presti, L.; Destro, R. Progress in the Understanding of the Key Pharmacophoric Features of the Antimalarial Drug Dihydroartemisinin: An Experimental and Theoretical Charge Density Study. *Chem.—A Eur. J.* **2013**, *19*, 3490−3503.
(19) Macetti, G.; Loconte, L.; Rizzato, S.; Gatti, C.; Lo Presti, L. Intermolecular Recognition of the Antimalarial Drug Chloroquine: A Quantum Theory of Atoms in Molecules-Density Functional Theory Investigation of the Hydrated Dihydrogen Phosphate Salt from the 103 K X-Ray Structure. *Cryst. Growth Des.* **2016**, *16*, 6043−6054.
(20) Zuccarello, F.; Buemi, G. A. A theoretical study of d-glucose, d-galactose, and parent molecules: solvent effect on conformational stabilities and rotational motions of exocyclic groups. *Carbohydr. Res.* **1995**, *273*, 129−145.
(21) Appell, M.; Strati, G.; Willett, J. L.; Momany, F. A. B3LYP/6-311++G** study of α- and β-d-glucopyranose and 1,5-anhydro-d-glucitol: 4C1 and 1C4 chairs, 3,OB and B3,O boats, and skew-boat conformations. *Carbohydr. Res.* **2004**, *339*, 537−551.
(22) Cramer, C. J.; Truhlar, D. G. Quantum Chemical Conformational Analysis of Glucose in Aqueous Solution. *J. Am. Chem. Soc.* **1993**, *115*, 5745−5753.
(23) Beyer, T.; Lewis, T.; Price, S. L. Which Organic Crystal Structures Are Predictable by Lattice Energy Minimisation? *CrystEngComm* **2001**, *3*, 178−212.
(24) van Eijck, B. P.; Mooij, W. T. M.; Kroon, J. Attempted Prediction of the Crystal Structures of Six Monosaccharides. *Acta Crystallogr.* **1995**, *51*, 99−103.
(25) van Eijck, B. P.; Kroon, J. UPACK Program Package for Crystal Structure Prediction: Force Fields and Crystal Structure Generation for Small Carbohydrate Molecules. *J. Comput. Chem.* **1999**, *20*, 799−812.
(26) Bader, R. F. W.*Atoms in Molecules. A Quantum Theory*, 1st ed.; Clarendon Press, Ed.; Oxford University Press: Oxford U.K., 1995.
(27) Bruker AXS Inc. *SAINT and SADABS. APEX II*, 2014.
(28) Altomare, A.; Cascarano, G.; Giacovazzo, C.; Guagliardi, A.; Burla, M. C.; Polidori, G.; Camalli, M.*SIR92 - a program for automatic solution of crystal structures by direct methods*; IUCr. urn:issn:0021-8898, 1994; Vol. *27* (3), pp 435.
(29) Sheldrick, G. M. A Short History of SHELX. *Acta Crystallogr., Sect. A: Found. Crystallogr.* **2008**, *64*, 112−122.
(30) Hansen, N. K.; Coppens, P. Testing Aspherical Atom Refinements on Small-Molecule Data Sets. *Acta Crystallogr., Sect. A: Cryst. Phys., Diffr., Theor. Gen. Crystallogr.* **1978**, *34*, 909−921.
(31) Volkov, A.; Macchi, P.; Farrugia, L. J.; Gatti, C.; Mallinson, P.; Richter, T.; Koritsanszky, T.*XD2016*. 2016.
(32) Clementi, E.; Roetti, C. Roothaan-Hartree-Fock Atomic Wavefunctions: Basis Functions and Their Coefficients for Ground and Certain Excited States of Neutral and Ionized Atoms, Z≤54. *At. Data Nucl. Data Tables* **1974**, *14*, 177−478.
(33) Allen, F. H.; Bruno, I. J. Bond lengths in organic and metal-organic compounds revisited:X-H bond lengths from neutron diffraction data. *Acta Crystallogr., Sect. B: Struct. Sci.* **2010**, *66*, 380−386.
(34) Madsen, A. Ø. SHADEweb server for estimation of hydrogen anisotropic displacement parameters. *J. Appl. Crystallogr.* **2006**, *39*, 757−758.
(35) Schomaker, V.; Trueblood, K. N. IUCr. On the Rigid-Body Motion of Molecules in Crystals. *Acta Crystallogr., Sect. B: Struct. Crystallogr. Cryst. Chem.* **1968**, *24*, 63−76.
(36) Lo Presti, L.; Gatti, C. Using the Source Function Descriptor to Dampen the Multipole Model Bias in Charge Density Studies from X-Ray Structure Factors Refinements. *Chem. Phys. Lett.* **2009**, *476*, 308−316.
(37) Gatti, C.; Lasi, D. Source Function Description of Metal−Metal Bonding in d-Block Organometallic Compounds. *Faraday Discuss.* **2007**, *135*, 55−78.
(38) Dovesi, R.; Erba, A.; Orlando, R.; Zicovich-Wilson, C. M.; Civalleri, B.; Maschio, L.; Rérat, M.; Casassa, S.; Baima, J.; Salustro, S.; et al. Quantum-Mechanical Condensed Matter Simulations with CRYSTAL. *Wiley Interdiscip. Rev.: Comput. Mol. Sci.* **2018**, *8*, No. e1360.
(39) Vilela Oliveira, D.; Laun, J.; Peintinger, M. F.; Bredow, T. BSSE-correction scheme for consistent gaussian basis sets of double- and triple-zeta valence with polarization quality for solid-state calculations. *J. Comput. Chem.* **2019**, *40*, 2364−2376.
(40) Adamo, C.; Barone, V. Toward Reliable Density Functional Methods without Adjustable Parameters: The PBE0 Model. *J. Chem. Phys.* **1999**, *110*, 6158.
(41) Gavezzotti, A.; Presti, L.; Rizzato, S. Molecular Dynamics Simulation of Organic Materials: Structure, Potentials and the MiCMoS Computer Platform. *CrystEngComm* **2022**, *24*, 922−930.
(42) Rizzato, S.; Gavezzotti, A.; Lo Presti, L. Molecular Dynamics Simulation of Molecular Crystals under Anisotropic Compression: Bulk and Directional Effects in Anthracene and Paracetamol. *Cryst. Growth Des.* **2020**, *20*, 7421−7428.
(43) Gavezzotti, A.; Lo Presti, L. Molecular Dynamics Simulation of Organic Crystals: Introducing the CLP-Dyncry Environment. *J. Appl. Crystallogr.* **2019**, *52*, 1253−1263.
(44) Gavezzotti, A.; Lo Presti, L.; Rizzato, S. Mining the Cambridge Database for theoretical chemistry. Mi-LJC: a new set of Lennard-Jones-Coulomb atom-atom potentials for the computer simulation of organic condensed matter. *CrystEngComm* **2020**, *22*, 7350−7360.
(45) Lo Presti, L.; Rizzato, S.; Gavezzotti, A. Kinetic-Bias Model for the Dynamic Simulation of Molecular Aggregation. The Liquid, Solute, Solvated-Nanodrop, and Solvated-Nanocrystal States of Benzoic Acid. *Cryst. Growth Des.* **2022**, *22* (3), 1857−1866.
(46) Lo Presti, L.; Gavezzotti, A.*MiCMoS - MIlano Chemistry MOlecular Simulation v2.0. MiCMoS User's Manual v2.0 2021*;

https://doi.org/10.1021/acs.cgd.2c00846
Cryst. Growth Des. 2022, 22, 6627−6638

Università degli Studi di Milano: Milano, 2021. https://sites.unimi.it/xtal_chem_group/index.php.
(47) Frisch, M. J.; Trucks, G. W.; Schlegel, H. B.; Scuseria, G. E.; Robb, M. A.; Cheeseman, J. R.; Scalmani, G.; Barone, V.; Mennucci, B.; Petersson, G. A.; et al.*Gaussian16*, Revision A.03); Gaussian Inc: Wallingford CT. Gaussian16 (Revision A.03), 2016.
(48) Boys, S. F.; Bernardi, F. The Calculation of Small Molecular Interactions by the Differences of Separate Total Energies. Some Procedures with Reduced Errors. *Mol. Phys.* **1970**, *19*, 553−566.
(49) Hamilton, W. C. Significance Tests on the Crystallographic R Factor. *Acta Crystallogr.* **1965**, *18*, 502−510.
(50) Destro, R.; Ruffo, R.; Roversi, P.; Soave, R.; Loconte, L.; Lo Presti, L. Anharmonic motions versus dynamic disorder at the Mg ion from the charge densities in pyrope (Mg3Al2Si3O12) crystals at 30 K: six of one, half a dozen of the other. *Acta Crystallogr., Sect. B: Struct. Sci., Cryst. Eng. Mater.* **2017**, *73*, 722−736.
(51) Destro, R.; Roversi, P.; Barzaghi, M.; Lo Presti, L. Anharmonic Thermal Motion Modelling in the Experimental XRD Charge Density Determination of 1-Methyluracil at T = 23 K. *Molecules* **2021**, *26*, 3075.
(52) Destro, R.; Presti, L.; Soave, R.; Goeta, A. E.Multi-Temperature Electron Density Studies. In *Modern Charge-Density Analysis*; Gatti, C., Macchi, P., Eds.; Springer Netherlands: Dordrecht, 2011, pp 659−696. DOI: 10.1007/978-90-481-3836-4_19
(53) Cremer, D.; Pople, J. A. General definition of ring puckering coordinates. *J. Am. Chem. Soc.* **1975**, *97*, 1354−1358.
(54) Spackman, M. A.; McKinnon, J. J. Fingerprinting Intermolecular Interactions in Molecular Crystals. *CrystEngComm* **2002**, *4*, 378−392.
(55) Spackman, M. A.; Jayatilaka, D. Hirshfeld Surface Analysis. *CrystEngComm* **2009**, *11*, 19−32.
(56) Meindl, K.; Henn, J. Foundations of Residual-Density Analysis. *Acta Crystallogr., Sect. A: Found. Crystallogr.* **2008**, *64*, 404−418.
(57) Meindl, K.; Herbst-Irmer, R.; Henn, J. On the Effect of Neglecting Anharmonic Nuclear Motion in Charge Density Studies. *Acta Crystallogr., Sect. A: Found. Crystallogr.* **2010**, *66*, 362−371.
(58) Destro, R.; Barzaghi, M.; Soave, R.; Roversi, P.; Lo Presti, L. Accurate experimental characterization of the labile N-Cl bond in N-chloro-N′-(p-fluorophenyl)-benzamidine crystal at 17.5 K. *CrystEngComm* **2022**, *24*, 6215−6225.
(59) van der Lee, A.; Dumitrescu, D. G. Thermal Expansion Properties of Organic Crystals: A CSD Study. *Chem. Sci.* **2021**, *12*, 8537−8547.
(60) Lo Presti, L.; Sist, M.; Loconte, L.; Pinto, A.; Tamborini, L.; Gatti, C. Rationalizing the Lacking of Inversion Symmetry in a Noncentrosymmetric Polar Racemate: An Experimental and Theoretical Study. *Cryst. Growth Des.* **2014**, *14*, 5822−5833.
(61) Lo Presti, L. On the Significance of Weak Hydrogen Bonds in Crystal Packing: A Large Databank Comparison of Polymorphic Structures. *CrystEngComm* **2018**, *20*, 5976−5989.
(62) Dunitz, J. D.; Gavezzotti, A. Molecular Recognition in Organic Crystals: Directed Intermolecular Bonds or Nonlocalized Bonding? *Angew. Chem., Int. Ed.* **2005**, *44*, 1766−1787.
(63) Gelbrich, T.; Braun, D. E.; Griesser, U. J. Specific Energy Contributions from Competing Hydrogen-Bonded Structures in Six Polymorphs of Phenobarbital. *Chem. Cent. J.* **2016**, *10*, 8.
(64) Abramov, Y. A. On the Possibility of Kinetic Energy Density Evaluation from the Experimental Electron-Density Distribution. *Acta Crystallogr., Sect. A: Found. Crystallogr.* **1997**, *53*, 264−272.
(65) Espinosa, E.; Molins, E.; Lecomte, C. Hydrogen Bond Strengths Revealed by Topological Analyses of Experimentally Observed Electron Densities. *Chem. Phys. Lett.* **1998**, *285*, 170−173.
(66) Gatti, C.; May, E.; Destro, R.; Cargnoni, F. Fundamental Properties and Nature of CH··O Interactions in Crystals on the Basis of Experimental and Theoretical Charge Densities. The Case of 3,4-Bis(dimethylamino)-3-cyclobutene-1,2-dione (DMACB) Crystal. *J. Phys. Chem. A* **2002**, *106*, 2707−2720.
(67) Saleh, G.; Gatti, C.; Lo Presti, L.; Contreras-García, J. Revealing Non-Covalent Interactions in Molecular Crystals through Their Experimental Electron Densities. *Chem.—A Eur. J.* **2012**, *18*, 15523−15536.
(68) Oliveira, L. B. A.; Colherinhas, G. TD-DFT and GIAO-NMR spectroscopy studies for maltose and (α- and β)-glucose in water solution using S-MC/QM polarization methodology. *J. Mol. Liq.* **2017**, *237*, 295−303.
(69) Mazurkiewicz, J.; Tomasik, P. Effect of External Electric Field upon Charge Distribution, Energy and Dipole Moment of Selected Monosaccharide Molecules. *Nat. Sci.* **2012**, *04*, 276−285.
(70) NEUROtiker. Glucose - Wikipedia. https://en.wikipedia.org/wiki/Glucose (accessed July 25, 2022).

https://doi.org/10.1021/acs.cgd.2c00846
Cryst. Growth Des. 2022, 22, 6627−6638